Environmental Science
Processes & Impacts

Accepted Manuscript

ROYAL SOCIETY OF CHEMISTRY

rsc.li/process-impacts

The interaction mechanisms between γ-Al_2O_3, Eu(III) and humic substances are greatly dependent on the temperature and contact order.

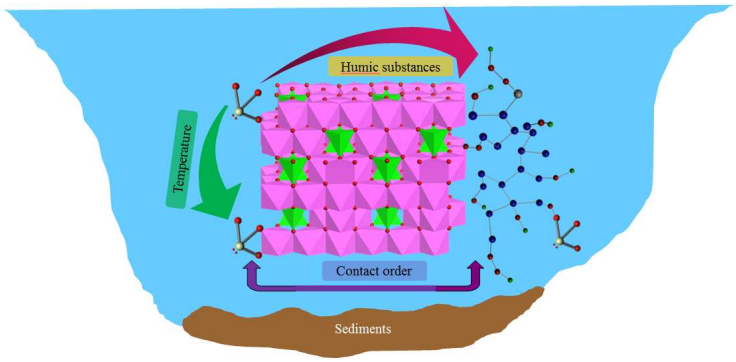

This study highlights the influence of temperature and contact order between γ-Al_2O_3, Eu(III) and humic acid (HA) on the sorption behaviors and sequestration mechanisms of Eu(III). The elevated temperature near the geological repository is beneficial to Eu(III) immobilization. In addition, the experimental findings suggest that the contact sequences between the radionuclides, humic substances and natural minerals should be taken into consideration so as to precisely understand the long-term behaviors of the radionuclides in the real geological environment. This work will help readers to understand the security of radioactive waste repositories and evaluate the fate of trivalent actinides (e.g., Am(III), Cm(III), Pu(III) and etc.) therein.

Sequestration and speciation of Eu(III) on gamma alumina: role of temperature and contact order

Yawen Cai [a, b], Xuemei Ren [c], Yue Lang [a, b], Zhiyong Liu [a, b], Pengfei Zong [d], Xiangke Wang [a, b], Shitong Yang [a, b]*

[a] School for Radiological and Interdisciplinary Sciences, Soochow University, 215123 Suzhou, P. R. China

[b] Collaborative Innovation Center of Radiation Medicine of Jiangsu Higher Education Institutions, 215123 Suzhou, P. R. China

[c] Institute of Plasma Physics, Chinese Academy of Sciences, P. O. Box 1126, 230031 Hefei, P. R. China

[d] Reactor Operation and Application Division, Nuclear Power Institute of China, 610005 Chengdu, P. R. China

*: Corresponding author. Email: shitongyang@suda.edu.cn; Tel: +86-512-65883945; Fax: +86-512-65883945.

Abstract. The speciation, migration and transport of radionuclides in the environment are significantly influenced by their interactions with the natural minerals and humic substances therein. In view of this, the effect of temperature and contact order on the sorption behaviors of trivalent Eu(III) in the γ-Al_2O_3/Eu(III) and γ-Al_2O_3/HA/Eu(III) systems were studied using the batch experiments and extended X-ray absorption fine structure spectroscopy (EXAFS) technique. The endothermic sorption behavior of Eu(III) in the γ-Al_2O_3/Eu(III) systems was induced by the hydrolysis reaction of Eu(III) in solution and the complexation of Eu(III) with the γ-Al_2O_3 surface sites. The

endothermic sorption of Eu(III) in the γ-Al_2O_3/HA/Eu(III) systems was attributed to the endothermic binding of HA on γ-Al_2O_3 and the endothermic complexation between Eu(III) and HA. EXAFS analysis suggested the formation of type B ternary complexes and their thermodynamic stability improves with rising temperature. The different sorption percentages under various contact orders were closely related with the binding mode of Eu(III) on the exposed γ-Al_2O_3 surfaces or the γ-Al_2O_3/HA colloids. The findings obtained herein are important to evaluate the security of the radioactive waste repository and predict the fate of trivalent actinides (e.g., Am(III), Cm(III), Pu(III) and etc.) near the geological repository.

Keywords: Eu(III); Temperature; Contact order; EXAFS; Sequestration mechanisms

1. Introduction

The deep geological landfill is an internationally-used approach for the disposition of radioactive wastes. With increased aging time, the toxic radionuclides may permeate through the multi-barriers and enter the surrounding soil and underground water systems. Depending on the specific environmental conditions, a series of chemical processes such as ion exchange, surface complexation, lattice incorporation, oxidation, reduction and precipitation can occur between the natural minerals, humic substances (e.g., humic acid (HA), fuvic acid (FA) and humin) and the radionuclides.[1-5] These interface interactions greatly influence the speciation, migration and transformation of radionuclides near the repository. Owing to its proper fluorescence yield, Eu(III) is often selected as a representative analogue for evaluating the environmental behaviors of trivalent actinides (e.g., Am(III) and Cm(III)) in the geologic environment.[6-11]

The temperature of the geological repository can rise up to 100 °C due to the radiative effects (e.g., disintegration or radiolysis) of the nuclear wastes.[12,13] According to the previous calculations, this elevated temperature would remain for a long period (~1000 years) and then slightly decrease to about 50 °C after another 1000 years.[14,15] In addition, the solution temperature for various environmental systems usually fluctuates with the changing of season and location. The variation in temperature could influence the hydrolysis behavior of radionuclides, the sorption dynamic of radionuclides at mineral/water interfaces, the complexation of radionuclides with humic substances and the thermodynamic stability of the formed species. For instance, the sorption behaviors of Eu(III) on hematite, amorphous ferric hydroxide, alumina, kaolinite, Na-montmorillonite and hydroxyapatite were reported to be endothermic on the basis of batch experiments, computational modeling, microcalorimetric titration, time resolved laser fluorescence spectroscopy (TRLFS) analysis and X-ray absorption spectroscopy (XAS) approach.[13,16-19] The observed endothermic phenomena were attributed to the dehydration upon surface binding and the enhanced surface complexation with increasing temperature. However, the sorption of Eu(III) on attapulgite, smectite and granite was not obviously influenced by the variation of temperature.[12,20,21] Moreover, the sorption of Eu(III) on calcareous soil and polyacylamide cerium titanate was reported to be an exothermic process.[22,23] In brief, the different effect of temperature variation on the sorption behaviors of Eu(III) at various solid/water interfaces may arise from the differences in the surface properties of the used sorbents and the experimental conditions (e.g., solution pH, temperature

range, hydrolysis reaction, and etc.).

Owing to the diversity and variability of the real aquatic environmental system, the chemical speciation and the migration trends of radionuclides are greatly dependent on their contact order with the natural minerals and humic substances therein. Previous studies showed that the sorption behaviors of trivalent lanthanides/actinides (e.g., Yb, Eu and Cm) in the ternary alumina/FA/Yb, attapulgite/HA/Eu, carbon nanotubes/HA/Eu, carbon nanotubes/PAA/Eu and montmorillonite/FA/Cm systems were disparate for different contact orders.[20,24-27] The diversity was interpreted by the irreversible sorption of HA/FA at the solid/water interfaces and the higher affinity of the adsorbed HA/FA towards these metal ions. However, Wang et al. reported that the chemical speciation of Cm(III) in the ternary alumina/HA/Cm(III) systems was not obviously influenced by the variation of contact order.[28] The authors proposed that the sorption of HA on the alumina surfaces was reversible and the adsorbed HA moieties possessed similar properties to those remaining in the solution. These incompatible findings and the controversial discussions may be induced by the physicochemical properties of the sorbents, the sources and nature of the HA/FA as well as the experimental conditions (e.g., solid/liquid ratio, solution pH, initial Eu(III)/Cm(III) concentration and etc.).

This work is an extension of our previous studies,[9,29] where we investigated the interaction mechanisms between Eu(III), HA and γ-Al_2O_3 as a function of reaction time, solution pH and ionic strength using batch and EXAFS techniques. The results suggested the formation of 1:1 (i.e., γ-Al_2O_3/L/Eu(III), L represents the binding sites

of adsorbed HA molecules) type B ternary complexes and binary corner-shared complexes at pH 6.5 with 2 d. With prolonged aging time, the formed type B ternary complexes tended to transfer into a 1:2 (i.e., γ-Al_2O_3/L_2/Eu(III)) linkage mode. In this study, the macroscopic sorption behaviors of Eu(III) in the γ-Al_2O_3/Eu(III) and γ-Al_2O_3/HA/Eu(III) systems were studied as a function of temperature and contact order by using the batch experiments. In addition, the microscopic species and the underlying sorption mechanisms were identified from the Eu(III) L_{III}-edge EXAFS spectroscopy. The obtained experimental findings were combined to further predict the migration and fate of trivalent lanthanides/actinides in the geological environment.

2. Experimental

2.1 Materials and reagents

The γ-Al_2O_3 powder used in the present study has a specific surface area of 100 m^2/g and a primary particle size of ~20 nm. The radiotracer $^{152+154}$Eu(III) (radiochemical purity ~99.0%) was purchased in the form of Eu_2O_3. The Eu(III) stock solution was prepared from the by dissolving, evaporating and re-dissolving the Eu_2O_3 powder in an diluted HNO_3 solution (0.001 mol/L). The HA sample was extensively investigated in our previous studies.[9,30,31] The other chemical reagent were purchased in analytical pure and used directly in the following experiments.

2.2 Batch experiments

The batch sorption of Eu(III) on γ-Al_2O_3 was investigated by using batch technique in 10-mL polyethylene centrifuge tubes under N_2 conditions. Briefly, the γ-Al_2O_3 suspensions, $NaNO_3$ solution, Eu(III) stock solution including trace quantities of the

radiotracer $^{152+154}$Eu(III) and/or the HA stock solution were added into the centrifuge tubes to achieve the desired concentrations. Specifically, the concentration of the $NaNO_3$ electrolyte solution was maintained constantly at 0.01 mol/L in all the sorption experiments. The pH values of the mixtures were adjusted with tiny amounts of HNO_3 or NaOH solutions. The resulting mixtures were shaken for 2 d and the solid was separated from the solution by centrifuging at 31152 ×*g*. The radioactivity of $^{152+154}$Eu(III) in the supernatant was measured by using the liquid scintillation counter. The sorption percentages of Eu(III) were then calculated from the total radioactivity of the $^{152+154}$Eu(III) (A_{tot}) in the initial solution and that remained in the supernatant (A_L) (i.e., Sorption%=$(1-A_L/A_{tot})\times100\%$).

2.3 EXAFS data collection and analysis

The Eu(III)-containing sorption samples for EXAFS analysis were prepared using a 250 mL vessel under various experimental conditions (see Table 1). Specifically, the Eu(III) stock solution was slowly added to the vessel under constant stirring to avoid the aggregation of Eu(III) ions. This procedure can exclude the formation of bulk hydroxide precipitate during the addition of Eu(III) stock solution. The suspension pH was monitored and maintained at the desired value during Eu(III) addition. After an aging time of 2 d, the suspensions were centrifuged at 31152 ×*g* for 20 min. The collected wet pastes were then wrapped in a moist paper towel and sealed in a Ziploc bag. To eliminate further interactions before the spectral measurements, the Ziploc bag was put in an airtight glass jar and settled in cold (3 ^{o}C) storage.

The Eu(III) L_{III}-edge EXAFS spectra were recorded at BL14W1 of Shanghai

Synchrotron Radiation Facility (SSRF, China). The collected EXAFS data were analyzed by using the Athena and Artemis software. Specifically, the EXAFS functions were weighted by k^3 and Fourier transformation was conducted within the k range of 2.0-11.0 $Å^{-1}$ to get the radial structural functions (RSFs). A nonlinear least-square fitting was then performed with the theoretical amplitude and phase parameters of reference $Eu(OH)_3(s)$, $[Eu(\mu\text{-}CH_3COO\text{-}O)(CH_3COO)_2(H_2O)_2]_2 \cdot 4H_2O$ and europium aluminum garnet ($Eu_3Al_5O_{12}$) generated by FEFF7.[32,33] The amplitude reduction factor (S_0^2) value was fixed at 1.0 to accurately reproduce the coordination numbers of neighboring atoms in the structure of the reference phases. The S_0^2 value set herein was consistent with the earlier studies on the coordination environment of lanthanides in the aqueous solution. During the fitting procedure, the coordination number (*CN*), bond distance (*R*) and Debye-Waller factor (σ^2) in the first coordination shell was set as variable factors. In contrast, the σ^2 values in the second coordination shell were fixed equal to that of $Eu(OH)_3(s)$ (i.e., 0.008 $Å^2$). The number of variable factors did not exceed the maximum limit of the Stern's rule.

3. Results and discussion

3.1 Batch experimental data

3.1.1 Effect of temperature on γ-Al_2O_3/Eu(III) systems

Figure 1 shows the sorption isotherms of Eu(III) in the γ-Al_2O_3/Eu(III) systems at four temperatures. The sorption amount of Eu(III) on γ-Al_2O_3 slightly increases with rising temperature, suggesting a weakly endothermic process. This experimental result is consistent with the weakly positive enthalpy change (11 kJ/mol) for Eu(III) sorption

on γ-Al_2O_3 as indicated by the microcalorimetric titration and surface complexation modeling.[8] It is reported that the γ-Al_2O_3 phase is not stable in the aqueous solution and would gradually convert into a transient amorphous phase and a bayerite-like crystallized phase.[34,35] In view of this, it is necessary to verify whether the endothermic process is attributed to the phase transition of the γ-Al_2O_3 substrate in solution. Herein, four individual γ-Al_2O_3 samples were soaked in the solution with different temperatures (viz. 293, 313, 333 and 353 K, respectively) for 2 d. Afterwards, the γ-Al_2O_3 solids were separated from the liquid phase and then dried for the XRD analysis. One can see from Figure 2 that no variation on the crystalline phase of γ-Al_2O_3 substrate occurs with rising solution temperatures. This phenomenon implies that the endothermic process of Eu(III) sorption is not due to the thermally induced phase-transition of the γ-Al_2O_3 substrate in solution. A previous study proposed that an aging time of 4 d is needed for the transformation of the γ-Al_2O_3 substrate into a new phase.[34] The aging time of 2 d in the present sorption systems is not sufficient for the transition of γ-Al_2O_3 phase. In view of this, one can speculate that the endothermic sorption feature herein is probably attributed to the hydrolysis reaction of Eu(III) in solution and the complexation of Eu(III) with the γ-Al_2O_3 sites.

To verify the contribution of the hydrolysis reaction, the relative proportion of Eu(III) species in solution is computed by using the Visual MINTEQ ver. 3.0.[36] As shown in Figure 3, Eu(III) in the solution is present as the Eu^{3+} ions and their first hydrolysis product (i.e., $EuOH^{2+}$) over a wide range of pH and temperature. At pH 6.5, the hydrated Eu^{3+} ions are the predominant species at 293 K. With increasing temperature,

more Eu^{3+} ions are submitted to the hydrolysis reaction and therefore increase the relative proportion of the $EuOH^{2+}$ species. According to the previous potentiometric and spectrophotometric measurements,[37] the formation constant (log*K*) for the $EuOH^{2+}$ species gradually increased from -8.14 at 288 K to -7.13 at 343 K. In view of this, one can deduce that the endothermic sorption of Eu(III) on the γ-Al_2O_3 surfaces is partly due to the hydrolysis reaction of Eu(III) in solution. Based on the surface complexation modeling, Quinn et al. proposed that the average enthalpy (10.4±1.2 kcal/mol) for Yttrium and rare earth elements sorption on amorphous ferric hydroxide value was similar to the average enthalpy for their hydrolysis reaction (~11.3 kcal/mol).[38] In general, the coordinated water molecules in the Eu(III) hydration shell is more ordered than the water located in the bulk γ-Al_2O_3 phase.[39] Hence, the loss of the coordinated water molecules upon surface complexation would result in the increased disorder of the sorption system. In addition, the disorder level of the water in the bulk γ-Al_2O_3 phase would increase with rising temperature. These two variation trends are consistent with the endothermic process for Eu(III) sorption on γ-Al_2O_3. From the standpoint of enthalpy change, the sorption of Eu(III) requires a diffusion process from the aqueous solution onto the γ-Al_2O_3 surfaces, which is an endothermic process. In addition, the loss of the coordinated water molecules from the primary hydration shell is the prelusion for the complexation of Eu(III) with the hydroxyl sites on the γ-Al_2O_3 surfaces.[18] This dehydration is also an endothermic process and is more favored at high temperature. Based on these experimental results, one can find that the elevated temperature is beneficial to the immobilization of Eu(III). It is

generally approved that the Eu(III) can be used as a chemical analogue of trivalent actinides (e.g., Am(III) and Cm(III)). However, some slight differences between their complexation ability with organic matter and sorption affinity to solid phases have been reported in the previous studies.[40-42] In view of this, one must take these disparities into consideration so as to precisely extrapolate the fate of trivalent actinides in the near field of the geological repository.

3.1.2 Effect of temperature on γ-Al_2O_3/HA/Eu(III) systems

To verify the influence of coexisting HA on Eu(III) binding behaviors, the sorption isotherms of Eu(III) in the ternary γ-Al_2O_3/HA/Eu(III) systems were also conducted at 293, 313, 333 and 353 K, respectively. As shown in Figure 4, the sorption amount of Eu(III) increases with increasing temperature. This phenomenon is indicative of an endothermic process for Eu(III) sorption in the γ-Al_2O_3/HA/Eu(III) systems. Herein, the endothermic sorption behavior is closely related with the increase of HA sorption on γ-Al_2O_3 surfaces with rising temperature (Figure 5). The augment in HA sorption at higher temperature would increase the amount of free carboxyl sites for binding Eu(III) and thus lead to the increase of Eu(III) sorption amount. Previous UV-vis spectroscopic study indicated that the rising in temperature could facilitate the deprotonation of HA carboxylic sites,[43] which correspondingly improve their binding affinity for Eu(III). The deprotonation reactions can also enhance the electrostatic repulsion among the HA moieties, leading to the formation of a stretched HA conformation. Under this circumstance, the carboxylic sites in the HA molecules are more available for binding Eu(III). Moreover, previous study implied that the

complexation between Eu(III) with simple carboxylic acid (e.g., acetic, propionic and succinic acid) was endothermic and the complexation affinity became stronger with rising temperature.[44] In view of this, the complexation of Eu(III) with HA (a kind of complex carboxylic acid) is expected to be endothermic.[45] The endothermic dehydration of Eu(III) hydration shell and the endothermic complexation between Eu(III) and HA lead to the endothermic behavior for Eu(III) sorption in the ternary γ-Al_2O_3/HA/Eu(III) systems. In addition, the endothermic process herein may be partly due to the hydrolysis reaction of Eu(III) in solution and the complexation of Eu(III) with the γ-Al_2O_3 surface sites as proposed for the binary γ-Al_2O_3/Eu(III) systems. As a result, the formation of binary surface complexes is expected under this circumstance. However, the binary surface complexes cannot be discriminated from the ternary surface complexes solely based on the macroscopic experimental data and further investigation (e.g., EXAFS analysis) is needed to obtain the microscopic sorption mechanisms.

3.1.3 Effect of contact order

The sorption behaviors of Eu(III) were investigated at pH 6.5 for the following four contact orders: (1) the γ-Al_2O_3, Eu(III) and HA stock solutions were simultaneously added into the vials and the resulting mixtures were gently oscillated for 2 d (batch 1); (2) the γ-Al_2O_3 and Eu(III) stock solutions were pre-equilibrated for 1 d, then the HA stock solution was added and the mixtures were gently oscillated for 1 d (batch 2); (3) the γ-Al_2O_3 and HA stock solutions were pre-equilibrated for 1 d, then the Eu(III) stock solution was added and the mixtures were gently oscillated for 1 d (batch 3);

and (4) the Eu(III) and HA stock solutions were pre-equilibrated for 1 d, then the γ-Al_2O_3 suspensions were added and the mixtures were gently oscillated for 1 d (batch 4). Note that the oscillating time for the four contact orders was kept at 2 d to eliminate its influence on the sorption behaviors.

As illustrated in Figure 6, the sorption percentage of Eu(III) on γ-Al_2O_3 exhibits a decreasing order of batch 3≈batch 1>batch 2>batch 4. This result can be tentatively interpreted by considering the binding of Eu(III) and/or HA on γ-Al_2O_3 surfaces, the complexation of Eu(III) with the surface-adsorbed HA moieties and the formation of HA-Eu(III) colloids in solution. For batch 3, the pre-added HA can be easily adsorbed on the positively charged γ-Al_2O_3 surfaces via ligand exchange reaction. The adsorbed HA substantially decrease the surface potential of the γ-Al_2O_3 substrate (Figure 7). This variation trend will create an expedient charge environment and consequently facilitates the close approach and attachment of positively charged Eu(III) ions. In addition, the decrease in the surface potentials of the γ-Al_2O_3 substrate by HA coating (i.e., increase in electrostatic repulsion) suggests that the γ-Al_2O_3/HA colloid could be well dispersed and suspended in the solution. Moreover, the surface-coated HA can effectively inhibit the aggregation of γ-Al_2O_3 particles in solution and protect the inner γ-Al_2O_3 substrate from dissolution. Hence, the dispersion and thermodynamic stability of γ-Al_2O_3 in the aquatic environments is greatly enhanced by the HA coating.[46] Under such circumstances, the subsequently added Eu(III) can be readily retained on the active sites of the γ-Al_2O_3 substrate and the surface-coated HA moieties. The sorption percentage of Eu(III) in batch 1 is comparable to that in batch 3, suggesting

the occurrence of similar sorption behaviors under these two different addition orders. It seems that the HA moieties in solution firstly bind on the γ-Al_2O_3 surfaces and then act as a ligand bridge between the Eu(III) ions and the γ-Al_2O_3 surfaces. The interaction between the γ-Al_2O_3 sites, the surface-coated HA moieties and the post-linked Eu(III) ions leads to the formation of type B ternary complexes. For batch 2, the pre-added Eu(III) tends to directly bind on the γ-Al_2O_3 hydroxyl sites, forming inner-sphere complexes. From the standpoint of charge environment, it seems more difficult for the approach of positively charged Eu(III) ions to the pure γ-Al_2O_3 surfaces (batch 2) than those to the HA-coated γ-Al_2O_3 surfaces (batch 3 and batch 1). In addition, the surface complexation procedure decreases the amount and availability of the hydroxyl sites for binding the subsequently added HA. As a result, more HA moieties are remained in solution and form soluble HA-Eu(III) complexes/colloids.[47] Owing to their strong complexation ability, the HA moieties in solution would desorb some Eu(III) ions that have been pre-adsorbed on the γ-Al_2O_3 surfaces. The aforementioned procedures competitively reduce the sorption percentage of Eu(III) on the γ-Al_2O_3 surfaces. For batch 4, the pre-equilibration between Eu(III) and HA in solution may facilitate the formation of HA-Eu(III) complexes. Herein, the concentration of Eu(III) and the amount of HA sites are quantitatively compared to determine the proportion of the formed HA-Eu(III) complexes. Theoretically, the amounts of carboxylic and phenolic sites in HA structure are calculated to be 2.44×10^{-5} mol/L and 6.0×10^{-6} mol/L by multiplying the HA mass concentration (herein, 10 mg/L) by the C content in the HA molecules (~60%) and by the previously

reported HA site contents.[20,48] According to the previous metal loading theory for lanthanides and HA complexation,[48-51] the Eu(III) ions tend to form complexes with the carboxylic sites in HA molecules under our experimental conditions (i.e., 10 mg/L of HA, 5.0×10^{-5} mol/L of Eu(III), pH 6.5). Herein, the concentration of Eu(III) ions in solution is almost double of the carboxylic amount in HA molecules. In view of this, ~ 50% of the initial Eu(III) in solution is present in the form of HA-Eu(III) complexes. Previous STXM, AFM, LSLM, TRLFS, PARAFAC and C 1s-NEXAFS analysis proposed that Eu(III) ions could cause HA agglomeration via intra- and intermolecular linkage and charge neutralization.[52-54] This phenomenon would further result in the formation of stable HA-Eu(III) colloids in solution with more compacted morphology, lower electronegativity, higher hydrophobicity and larger particle size relative to the free HA. These features inhibit the binding of HA-Eu(III) colloids on the subsequently added γ-Al_2O_3 surfaces. In addition, the bridging interactions between Eu(III) ions and the carboxylic sites would cause the formation of internal hydrophobic cavum in the HA structure. Compared with the hydrated Eu(III) ions, the HA-Eu(III) colloids with hydrophobic domains are more difficult to bind on the hydrophilic surface sites of γ-Al_2O_3. This is the tentative interpretation for the decrease of Eu(III) sorption percentage under this contact order.

3.2 EXAFS Analysis of Eu(III)-loaded samples

3.2.1 Effect of temperature on γ-Al_2O_3/Eu(III) systems

The k^3-weighted EXAFS spectra of the γ-Al_2O_3/Eu(III) samples prepared at different temperatures are shown in Figure 8A. One can see that the oscillation signals at k>6.3

Å^{-1} are obviously different from those of the Eu(III)(aq) and Eu(OH)$_3$(s) reference samples. This phenomenon suggests that the coordination environment of Eu(III) in the sorption samples is neither the hydrated ions nor the bulk hydroxide precipitate phase. Alternatively, the spectral features herein are probably resulted from the backscattering of the neighboring Al atoms surrounding the central Eu atom, pointing to the formation of inner-sphere complexes. Some slight changes in the spectral signals can be observed for different temperatures. Specifically, the intensity of the oscillation signal at ~8.4 Å^{-1} becomes more conspicuous with rising temperature (marked in the red box), while that of the oscillation signal at ~10.6 Å^{-1} shows a decreasing trend with rising temperature (marked in the blue box). This variation trend suggests that there exist two kinds of surface complexes and their relative proportion changes with increasing temperature.

The k^3-weighted spectra are Fourier transformed to illustrate the corresponding radial structure functions (RSFs) (Figure 8B). Apart from the main peak located at ~1.9 Å (phase shift uncorrected) that corresponds to the first Eu-O coordination shells, the RSFs for the four temperature-dependent samples exhibit an additional peak at ~3.2 Å. This spectral feature points to the appearance of higher coordination shells (e.g., the Eu-Al and/or Eu-Eu backscattering paths). However, the location and intensity of this peak is obviously different from those for the Eu(OH)$_3$(s) sample, which excludes the potential contribution of the Eu-Eu backscattering path. Alternatively, this peak is probably induced by the Eu-Al backscattering paths due to the surface complexation. One can see from Figure 8B that the intensity of this peak increases with rising

temperature (marked in the red box), which suggests an increasing contribution from the backscattering atoms with rising temperature.[9,29,31,55]

The experimental RSFs of the four samples can be successfully fitted by using the combination of one Eu-O backscattering path and two Eu-Al backscattering paths. The structural parameters derived from the nonlinear least-square fitting of the RSFs are listed in Table 2. The presence of surrounding Al atoms (i.e., $R_{\text{Eu-Al1}}$ ~3.27 Å and $R_{\text{Eu-Al2}}$ ~3.98 Å) in the second coordination shell manifests the formation of inner-sphere complexes. Based on the previous geometry calculations,[9] the shorter $R_{\text{Eu-Al1}}$ at ~3.27 Å correspond to the binding of Eu(III) on AlO_6 octahedra in an edge-shared mode (Figure 9), while the longer $R_{\text{Eu-Al2}}$ at ~3.98 Å correspond to the binding of Eu(III) on AlO_6 octahedra in a corner-shared mode (Figure 9). Herein, the edge-shared mode requires that the dehydrated Eu(III) ions coordinate with two surface hydroxyl sites on an individual AlO_6 octahedra, forming a tight geometric coordination structure. In contrast, the Eu-O polyhedra for the corner-shared mode are more flexible for binding on the individual AlO_6 octahedra.[56] Correspondingly, the longer Eu-Al bond in the corner-shared mode is weaker than the shorter Eu-Al bond in the edge-shared mode.[57] It is clear that the $CN_{\text{Eu-Al1}}$ at ~3.27 Å (corresponding to a strong edge-shared binding mode) increases with rising temperature, while the $CN_{\text{Eu-Al2}}$ at ~3.98 Å (corresponding to a weak corner-shared binding mode) decreases with rising temperature. The γ-Al_2O_3 phase contains two kinds of surface hydroxyl sites, i.e., the weak sites with high density and low sorption affinity as well as the strong sites with low density and high sorption affinity.[58-60] Note that the weak/strong

bindings described herein do not correspond to the weak/strong sites as assumed in the previous surface complexation modeling.[58-60] Objectively speaking, the EXAFS technique cannot distinguish the weak and strong surface sites located on the different crystal planes of γ-Al_2O_3 phase. Additional analysis approach, e.g., the bond-valence model,[61-63] is needed to further verify the specific surface sites for Eu(III) binding.

The reversibility for Eu(III) sorption on the γ-Al_2O_3 surfaces is greatly dependent on the specific binding mode and the thermodynamic stability of the adsorbed species. In general, the formation of inner-sphere complexes can substantially alter the solid surface structure, which is expected to decrease the sorption reversibility. Specifically for the two linkage modes of the inner-sphere complexation, the coordination bond for the edge-shared mode is stronger than for the corner-shared mode. In view of this, the adsorbed species in an edge-shared mode is more stable and less reversible than those in a corner-shared mode.[9,29,31,64-67] Hence, the sorption reversibility of Eu(III) on the γ-Al_2O_3 surfaces can be deduced from the relative ratio between the edge-shared and corner-shared linkages. Based on the structural parameters listed in Table 2, one can calculate that the ratio of $CN_{Eu\text{-}Al1}/CN_{Eu\text{-}Al2}$ increases from 0.65 to 1.31 as the temperature increases from 293 K to 353 K. This result indicates that the increased sorption amount and the decreased reversibility at higher temperature is closely related with the increased proportion of edge-shared binding as well as the decreased proportion of corner-shared binding. Herein, the tight immobilization of the Eu(III) ions on the γ-Al_2O_3 surfaces at higher temperature would significantly reduce their migration and the ecological risk in environmental mediums.

3.2.2 Effect of temperature on γ-Al_2O_3/HA/Eu(III) systems

Figure 10 shows the k^3-weighted EXAFS spectra (A) and the corresponding RSFs (B) of the γ-Al_2O_3/HA/Eu(III) samples prepared at various temperatures. One can see that the spectra are obviously different from those of the γ-Al_2O_3/Eu(III) samples (Figure 8A), suggesting the occurrence of difference sorption mechanisms for these two systems. In contrast, the oscillation signals are more analogous to the HA/Eu(III)(aq) sample (e.g., the beat feature at ~4.7 $Å^{-1}$ as marked in the gray boxes and the two broad peaks in the range of ~7.2-10.3 $Å^{-1}$). The comparability herein suggests that the sorption in the γ-Al_2O_3/HA/Eu(III) systems is dominated by the complexation between HA and Eu(III).[68] Nonetheless, some more oscillation signals appear in the EXAFS spectra of the γ-Al_2O_3/HA/Eu(III) samples relative to the HA/Eu(III)(aq) sample. For instance, the new oscillation feature at ~10.6 $Å^{-1}$ (as marked in the green boxes) points to the formation of additional surface complexes. In addition, the split of the oscillation peak at ~8.0 $Å^{-1}$ becomes more evident (marked in the red box) at higher temperatures (herein, 333 K and 353 K).

As shown in Figure 10B, an additional peak at ~3.2 Å (marked in the red box) appears in the RSFs of the four samples, pointing to the presence of backscattering atoms (e.g., C and/or Al) surrounding the central Eu atoms. It is worth noting that the intensity of this peak (i.e., ~3.2 Å) is slight lower than that of the γ-Al_2O_3/Eu(III) systems (Figure 8B). This diversity suggests that the second coordination shells of the central Eu atoms in the γ-Al_2O_3/HA/Eu(III) samples are probably due to the backscattering of lighter C atoms. This deduction is further supported by the successful fitting of the

RSFs with one Eu-C (~2.70 Å) and one longer Eu-Al (~3.98 Å) backscattering paths. Herein, the Eu-C bond at ~2.70 Å is attributed to the binding of Eu(III) with the functional groups of HA, forming type B ternary surface complexes (Figure 9).[9,68] The Eu-Al bond at ~3.98 Å suggests that some of the Eu(III) ions tend to directly coordinate with the active hydroxyl sites on the γ-Al_2O_3 surfaces, leading to the formation of binary corner-shared complexes (Figure 9). As listed in Table 2, the structural parameters for the four temperature-dependent samples can be divided into two groups depending on the $CN_{Eu\text{-}C}$ values, i.e., the samples prepared at lower temperatures (293 K and 313 K) with an average $CN_{Eu\text{-}C}$ value of ~1.4 and those prepared at higher temperatures (333 K and 353 K) with an average $CN_{Eu\text{-}C}$ value of ~2.2. This variation trend manifests that the stoichiometric ratio between Eu(III) and the C-containing sites (e.g., carboxyl, denoted as L) of the adsorbed HA increases from 1:1 (γ-Al_2O_3/L/Eu(III)) to 1:2 (γ-Al_2O_3/L_2/Eu(III)) with increasing temperature. Herein, the 1:2 ternary complexes are more thermodynamically stable and less reversible due to a stronger coordination linkage.[9,29]

3.2.3 Effect of contact order on γ-Al_2O_3/HA/Eu(III) systems

Figure 11 shows the k^3-weighted EXAFS spectra (A) and the corresponding RSFs (B) for the ternary γ-Al_2O_3/HA/Eu(III) samples prepared at different contact orders. As shown in Figure 11A, the spectra of batch 1 and batch 3 are quite similar to that of the HA/Eu(III)(aq) sample (e.g., the beat feature at ~4.7 $Å^{-1}$ as marked in the gray boxes and the two broad peaks in the range of ~7.2-10.3 $Å^{-1}$ as marked in the red boxes). This phenomenon suggests that Eu(III) tends to form complexes with the adsorbed

HA moieties for these two contact orders. In addition, the spectra for batch 1 and batch 3 show a new oscillation signal at ~10.6 $Å^{-1}$ (marked in the blue boxes), which points to the presence of another sorption complexes on the γ-Al_2O_3 surfaces. In contrast, the spectra of batch 2 and batch 4 are extremely similar to that of the binary γ-Al_2O_3/Eu(III) system (Figure 8A), suggesting an analogous sorption mechanism between these systems. The spectral differences between the four contact orders may arise from the backscattering of different atoms surrounding the central Eu atoms.

From the RSFs as illustrated in Figure 11B, one can see that the first peak at ~1.9 Å is quite similar for all the four sorption samples. However, some difference can be observed for the intensity of the peak located at ~3.2 Å. Although the Eu(III) sorption percentage in batch 1 and batch 3 is higher than that in batch 2 and batch 4 (Figure 6), the intensity of this peak at ~3.2 Å for batch 1 and batch 3 is lower than that for batch 2 and batch 4. In view of this, one can deduce that the central Eu atoms in batch 1 and batch 3 are surrounded by low-atomic-weight backscattering atoms. The experimental RSFs are seriatim fitted on the basis of the theoretically generated amplitude and phase functions. For batch 1 and batch 3, the central Eu atoms are coordinated with ~8.8 O atoms at $R_{Eu\text{-}O}$ ~2.40 Å, ~1.4 C atoms at $R_{Eu\text{-}C}$ ~2.71 Å and ~1.1 Al atoms at $R_{Eu\text{-}Al2}$ ~3.98 Å (Table 2). These structural parameters manifest that Eu(III) ions in batch 1 and batch 3 coordinate with the adsorbed HA and partly bind on the γ-Al_2O_3 hydroxyl sites,[9,29] forming type B ternary complexes and binary corner-shared complexes (Figure 9). In contrast, the structural parameters for batch 2 and batch 4 are comparable to those of the binary γ-Al_2O_3/Eu(III) sample (Table 2). The similarity

herein manifests that the sorption mechanism in batch 2 and batch 4 is attributed to the direct binding of Eu(III) on the γ-Al_2O_3 sites. Herein, the binary γ-Al_2O_3/Eu(III) surface complexes formed in batch 2 and batch 4 are disparate from the ternary γ-Al_2O_3/HA/Eu(III) surface complexes that dominate in batch 1 and batch 3. Based on the foregoing analysis, one can conclude that the diverse Eu(III) sorption percentages under various contact orders are induced by the different binding mode of Eu(III) on the exposed γ-Al_2O_3 surfaces or the γ-Al_2O_3/HA colloids.

4. Conclusions

This study highlights the influence of temperature and contact order between the γ-Al_2O_3, Eu(III) and HA on the macroscopic sorption behaviors and the microscopic sequestration mechanisms of Eu(III). Considering that Eu(III) is extensively selected as a representative analogue for the trivalent actinides (e.g., Am(III), Cm(III), Pu(III) and etc.), the experimental findings herein could provide important data for assessing the security of the high-level radioactive waste repository and evaluating the fate of these actinides. The batch experiments showed that the sorption of Eu(III) in the both the γ-Al_2O_3/Eu(III) and γ-Al_2O_3/HA/Eu(III) systems increased with rising temperature. EXAFS analysis implied that the endothermic sorption of Eu(III) in the binary γ-Al_2O_3/Eu(III) systems was due to the increased contribution of stronger edge-shared surface complexes and the decreased contribution of weaker corner-shared complexes. Dissimilarly, EXAFS analysis suggested the formation of type B ternary complexes in the γ-Al_2O_3/HA/Eu(III) systems and the thermodynamic stability of the formed complexes improved with rising temperature. According to these results, one can

deduce that the elevated temperature in the near field of the repository is beneficial to the immobilization of trivalent actinides. The different sorption percentages under various contact orders were induced by the disparate linkage mode of Eu(III) on the exposed γ-Al_2O_3 surfaces or the γ-Al_2O_3/HA colloids. In view of this, the contact orders between the radionuclides, humic substances and the natural minerals should be taken into consideration so as to precisely understand the long-term behaviors of the radionuclides in the real environment.

Acknowledgements

Financial supports from Natural Science Foundation of China (41203086), Jiangsu Provincial Key Laboratory of Radiation Medicine and Protection and the Priority Academic Program Development of Jiangsu Higher Education Institutions (PAPD) are acknowledged. We thank Prof. Yuying Huang, Zheng Jiang, Xiangjun Wei and Dr. Jingyuan Ma of SSRF for their technical assistance in the EXAFS data collection.

References

1 M. H. Bradbury, B. Baeyens, H. Geckeis and T. Rabung, *Geochim. Cosmochim. Acta*, 2005, **69**, 5403-5412.

2 P. Mandaliev, T. Stumpf, J. Tits, R. Dähn, C. Walther and E. Wieland, *Geochim. Cosmochim. Acta*, 2011, **75**, 2017-2029.

3 N. D. Bryan, L. Abrahamsen, N. Evans, P. Warwick, G. Buckau, L. Weng and W. H. Van Riemsdijk, *Appl. Geochem.*, 2012, **27**, 378-389.

4 H. Geckeis, J. Lützenkirchen, R. Polly, T. Rabung and M. Schmidt, *Chem. Rev.*, 2013, **113**, 1016-1062.

5 R. Marsac, N. L. Banik, J. Lützenkirchen, C. M. Marquardt, K. Dardenne, D. Schild, J. Rothe, A. Diascorn, T. Kupcik, T. Schäfer and H. Geckeis, *Geochim. Cosmochim. Acta*, 2015, **152**, 39-51.

6 T. Stumpt, H. Curtius, C. Walther, K. Dardenne, K. Ufer and T. Fanghänel, *Environ. Sci. Technol.*, 2007, **41**, 3186-3191.

7 J. Brevet, F. Claret and P. E. Reiller, *Spectrochim. Acta A*, 2009, **74**, 446-453.

8 J. P. Morel, N. Marmier, C. Hurel and N. Morel-Desrosiers, *J. Colloid Interface Sci.*, 2012, **376**, 196-201.

9 S. T. Yang, G. D. Sheng, G. Montavon, Z. Q. Guo, X. L. Tan, B. Grambow and X. K. Wang, *Geochim. Cosmochim. Acta*, 2013, **121**, 84-104.

10 P. K. Verma, P. N. Pathak, P. K. Mohapatra, S. V. Godbole, R. M. Kadam, A. A. Veligzhanin, Y. V. Zubavichus and S. N. Kalmykov, *Environ. Sci.: Proc. Imp.*, 2014, **16**, 904-915.

11 G. Montavon, T. Rabung, H. Geikeis and B. Grambow, *Environ. Sci. Technol.*, 2004, **38**, 4312-4318.

12 A. Bauer, T. Rabung, F. Claret, T. Schäfer, G. Buckau and T. Fanghänel, *Appl. Clay Sci.*, 2005, **3**0, 1-10.

13 E. Tertre, G. Berger, E. Simoni, S. Castet, E. Giffaut, M. Loubet and H. Catalette, *Geochim. Cosmochim. Acta*, 2006, **70**, 4563-4578.

14 L. Ageskok and P. Janson, *SKB Technical Report*, Stockholm, Sweden, 1999.

15 J. W. Johnson, M. Niemeyer, G. Klubergans, P. Siegel and P. Gribi, *NTB 01-04*, Nagra, Wettingen, 2002.

16 K. Ishida, T. Kimura, T. Saito and S. Tanaka, *Environ. Sci. Technol.*, 2009, **43**, 1744-1749.

17 F. Granados-Correa, J. Vilchis-Granados, M. Jiménez-Reyes and L. A. Quiroz-Granados, *J. Chem.*, 2013, **1**, 1-9.

18 S. L. Estes, Y. Arai, U. Becker, S. Fernando, K. Yuan, R. C. Ewing, J. M. Zhang, T. Shibata and B. A. Powell, *Geochim. Cosmochim. Acta*, 2013, **122**, 430-447.

19 E. Tertre, G. Berger, S. Castet, M. Loubet and E. Giffaut, *Geochim. Cosmochim. Acta*, 2005, **69**, 4937-4948.

20 Q. H. Fan, X. L. Tan, J. X. Li, X. K. Wang, W. S. Wu and G. Montavon, *Environ. Sci. Technol.*, 2009, **43**, 5776-5782.

21 Q. Jin, G. Wang, M. T. Ge, Z. Y. Chen, W. S. Wu and Z. J. Guo, *Appl. Geochem.*,

2014, **47**, 17-24.

22 Y. Q. Wang, Q. H. Fan, P. Li, X. B. Zheng, J. Z. Xu, Y. R. Jin and W. S. Wu, *J. Radioanal. Nucl. Ch.*, 2011, **287**, 231-237.

23 I. M. El-Naggar, G. M. Ibrahim, E. A. El-Kady and E. A. Hegazy, *Desalination*, 2009, **237**, 147-154.

24 X. K. Wang, W. M. Dong, X. X. Dai, A. X.Wang, J. Z. Du and Z.Y. Tao, *Appl. Radiat. Isot.*, 2000, **52**, 165-173.

25 Y. Takahashi, T. Kimura and Y. Minai, *Geochim. Cosmochim. Acta*, 2002, **66**, 1-12.

26 Q. H. Fan, D. D. Shao, J. Hu, C. L. Chen, W. S. Wu and X. K. Wang, *Radiochim. Acta*, 2009, **97**, 1-8.

27 C. L. Chen, X. K. Wang and M. Nagatsu, *Environ. Sci. Technol.*, 2009, **43**, 2362-2367.

28 T. Rabung, H. Geckeis, P. J. Panak, R. Klenze and T. Fanghänel, *Radiochim. Acta*, 2004, **92**, 691-695.

29 S. T. Yang, P. F. Zong, G. D. Sheng, X. M. Ren, Y. Y. Huang and X. K. Wang, *Radiochim. Acta*, 2014, **102**, 143-153.

30 X. L. Tan, X. K. Wang, H. Geckeis and T. Rabung, *Environ. Sci. Technol.*, 2008, **42**, 6532-6537.

31 S. T. Yang, G. D. Sheng, X. L. Tan, J. Hu, J. Z. Du, G. Montavon and X. K. Wang, *Geochim. Cosmochim. Act*a, 2011, **75**, 6520-6534.

32 A. L. Ankudinov and J. J. Rehr, *Phys. Rev. B*, 1997, **56**, 1712-1715.

33 E. Garskaite, S. Sakirzanovas, A. Kareiva, J. Glaser and H. J. Meyer, *Z. Anorg. Allg. Chem*., 2007, **633**, 990-993.

34 G. Lefèvre, M. Duc, P. Lepeut, R. Caplain and M. Fédoroff, *Langmuir*, 2002, **1**8, 7530-7537.

35 X. Carrier, E. Marceau, J.F. Lambert and M. Che, *J. Colloid Interface Sci.*, 2007, **308**, 429-437.

36 J. P. Gustafsson, *Visual MINTEQ ver. 3.0*, Department of Land and Water Resources Engineering, KTH, SE-100 44, Stockholm, Sweden. Available at http://www2.lwr.kth.se/English/OurSoftware/vminteq/index.htm.

37 G. D. Klungness and R. H. Byrne, *Polyhedron*, 2000, **19**, 99-107.

38 K. A. Quinn, R. H. Byrne and J. Schijf, *Environ. Sci. Technol.*, 2007, **41**, 541-546.

39 G. E. Brown, Jr., V. E. Henrich, W. H. Casey, D. L. Clark, C. Eggleston, A. Felmy, D. W. Goodman, M. Grätzel, G. Maciel, M. I. McCarthy, K. H. Nealson, D. A. Sverjensky, M. F. Toney and J. M. Zachara, *Chem. Rev.*, 1999, **99**, 77-174.

40 T. Kimura, Y. Kato, H. Takeishi and G. R. Choppin, *J. Alloy. Compd.*, 1998, **271-273**, 719-722.

41. Q. H. Fan, M. L. Zhang, Y. Y. Zhang, K. F. Ding, Z. Q. Yang and W. S. Wu, *Radiochim. Acta*, 2010, **98**, 19-25.

42 Q. H. Fan, X. L. Zhao, X. X. Ma, Y. B. Yang, W. S. Wu, G. D. Zheng and D. L. Wang, *Environ. Sci.: Proc. Imp.*, 2015, **17**, 1634-1640.

43 M. Brigante, G. Zanini and M. Avena, *Colloid. Surf. A*, 2007, **294**, 64-70.

44 G. X. Tian, L. R. Martin and L. F. Rao, *Inorg. Chem.*, 2010, **49**, 10598-10605.

45 H. Baker and F. Khalili, *Ann. Environ. Sci.*, 2007, **1**, 35-44.

46 K. Yang, D. H. Lin and B. S. Xing, *Langmuir*, 2009, **25**, 3571-3576.

47 M. Davranche, O. Pourret, G. Gruau, A. Dia, D. Jin and D. Gaertner, *Chem. Geol.*, 2008, **247**, 154-170.

48 J. D. Ritchie and E. M. Perdue, *Geochim. Cosmochim. Acta*, 2003, **67**, 85-96.

49 J. C. Stern, J. E. Sonke and V. J. M. Salters, *Chem. Geol.*, 2007, **246**, 170-180.

50 R. Marsac, M. Davranche, G. Gruau and A. Dia, *Geochim. Cosmochim. Acta*, 2010, **74**, 1749-1761.

51 R. Marsac, M. Davranche, G. Gruau, A. Dia and M. Bouhnik-Le Coz, *Geochim. Cosmochim. Acta*, 2002, **89**, 1-9.

52 M. Plaschke, J. Rothe, T. Schäfer, M. A. Denecke, K. Dardenne, S. Pompe and K. H. Heise, *Colloid. Surf. A*, 2002, **197**, 245-256.

53 A. Naber, M. Plaschke, J. Rothe, H. Hofmann and T. Fanghänel, *J. Electron. Spectrosc. Relat. Phenom.*, 2006, **153**, 71-74.

54 I. Christl and R. Kretzschmar, *Environ. Sci. Technol.*, 2007, **41**, 1915-1920.

55 S. T. Yang, X. M. Ren, G. X. Zhao, W. Q. Shi, G. Montavon, B. Grambow and X. K. Wang, *Geochim. Cosmochim. Acta*, 2015, **166**, 129-145.

56 S. Kumar, A. S. Kar, B. S. Tomar and D. Bhattacharyya, *Polyhedron*, 2012, **33**, 33-40.

57 G. D. Sheng, S. T. Yang, Y. M. Li, X. Gao, Y. Y. Huang, J. Hu and X. K. Wang, *Radiochim. Acta*, 2014, **102**, 155-167.

58 T. Rabung, T. Stumpf, H. Geckeis, R. Klenze and J. I. Kim, *Radiochim. Acta*, 2000, **88**, 711-716.

59 T. Stumpf, T. Rabung, R. Klenze, H. Geckeis and J. I. Kim, Spectroscopic study of Cm(III) sorption onto γ-alumina. *J. Colloid Interface Sci.*, 2001, **238**, 219-224.

60 X. K. Wang, X. Zhou, J. Z. Du, W. P. Hu, C. L. Chen and Y. X. Chen, *Surf. Sci.*, 2006, **600**, 478-483.

61 J. R. Bargar, G. E. Brown, Jr. and G. A. Parks, *Geochim. Cosmochim. Acta*, 1997, **61**, 2617-2637.

62 G. A. Waychunas, C. C. Fuller and J. A. Davis, *Geochim. Cosmochim. Acta*, 2002, **66**, 1119-1137.

63 S. K. Ghose, G. A. Waychunas, T. P. Trainor and P. J. Eng, *Geochim. Cosmochim. Acta*, 2010, **74**, 1943-1953.

64 E. J. Elzinga and R. J. Reeder, *Geochim. Cosmochim. Acta*, 2002, **66**, 3943-3954.

65 G. Pan, Y. W. Qin, X. L. Li, T. D. Hu, Z. Y. Wu and Y. N. Xie, *J. Colloid Interface Sci.*, 2004, **271**, 28-34.

66 X. L. Li, G. Pan, Y. W. Qin, T. D. Hu, Z. Y. Wu and Y. N. Xie, *J. Colloid Interface Sci.*, 2004, **271**, 35-40.

67 W. Li, G. Pan, M. Zhang, D. Zhao, Y. Yang, H. Chen and G. He, *J. Colloid Interface Sci.*, 2008, **319**, 385-391.

68 G. D. Sheng, Q. Yang, F. Peng, H. Li, X. Gao, Y. Y. Huang, *Chem. Eng. J.*, 2014, **245**, 10-16.

Table 1 Experimental conditions for the EXAFS analysis of Eu(III)-containing samples. t=2 *d*, pH=6.5, m/V=0.5 g/L, $C_{Eu(III)initial}$=5×10^{-5} mol/L, *I*=0.01 mol/L $NaNO_3$.

Sample conditions		$C_{(HA)initial}$ (mg/L)	Sorption percentage (%)	Sorption amount (μmol/g)
γ-Al_2O_3/Eu(III) binary system	*T*=293 K	0	64	64
	T=313 K	0	70	70
	T=333 K	0	74	74
	T=353 K	0	77	77
γ-Al_2O_3/HA/Eu(III) ternary system	*T*=293 K	10	73	73
	T=313 K	10	76	76
	T=333 K	10	80	80
	T=353 K	10	83	83
	Batch 1	10	73	73
	Batch 2	10	62	62
	Batch 3	10	72	72
	Batch 4	10	48	48

Table 2 The structural parameters derived from the EXAFS analysis for Eu(III)-containing reference and sorption samples.

Sample conditions		First shell (Eu-O)			Second shell (Eu-C/Al/Eu)				
		R (Å)	*CN*	σ^2 (Å^2)	Bond	*R* (Å)	*CN*	σ^2 (Å^2)	R_f
Reference samples	Eu(III)(aq)	2.41	8.8	0.004					0.057
	HA/Eu(III)(aq)	2.40	8.6	0.005	Eu-C	2.70	1.4	*0.008*	0.065
	$Eu(OH)_3$(s)	2.40	8.5	0.004	Eu-Eu	3.65	2.2	*0.008*	0.030
γ-Al_2O_3/Eu(III) binary system pH=6.5	*T*=293 K	2.41	8.7	0.005	Eu-Al1	3.27	1.7	*0.008*	0.062
					Eu-Al2	3.99	2.6	*0.008*	
	T=313 K	2.40	8.5	0.004	Eu-Al1	3.25	1.8	*0.008*	0.055
					Eu-Al2	3.98	2.2	*0.008*	
	T=333 K	2.42	8.3	0.005	Eu-Al1	3.26	2.0	*0.008*	0.059
					Eu-Al2	3.40	1.8	*0.008*	
	T=353 K	2.39	8.4	0.007	Eu-Al1	3.26	2.1	*0.008*	0.047
					Eu-Al2	3.99	1.6	*0.008*	
γ-Al_2O_3/HA/Eu(III) ternary system pH=6.5	*T*=293 K	2.40	8.9	0.003	Eu-C	2.70	1.3	*0.008*	0.052
					Eu-Al2	3.98	1.1	*0.008*	
	T=313 K	2.41	8.7	0.004	Eu-C	2.69	1.5	*0.008*	0.048
					Eu-Al2	3.99	1.0	*0.008*	
	T=333 K	2.42	8.5	0.006	Eu-C	2.71	2.1	*0.008*	0.037
					Eu-Al2	3.97	1.2	*0.008*	
	T=353 K	2.42	8.6	0.007	Eu-C	2.70	2.3	*0.008*	0.023
					Eu-Al2	3.98	1.1	*0.008*	
γ-Al_2O_3/HA/Eu(III) ternary system pH=6.5	Batch 1	2.41	8.8	0.003	Eu-C	2.71	1.5	*0.008*	0.047
					Eu-Al2	3.98	1.0	*0.008*	
	Batch 2	2.39	8.6	0.006	Eu-Al1	3.27	1.6	*0.008*	0.061
					Eu-Al2	3.98	2.4	*0.008*	
	Batch 3	2.40	8.9	0.003	Eu-C	2.70	1.3	*0.008*	0.052
					Eu-Al2	3.98	1.1	*0.008*	
	Batch 4	2.39	8.7	0.006	Eu-Al1	3.28	1.4	*0.008*	0.038
					Eu-Al2	3.99	2.3	*0.008*	

R--Bond distance, *CN*--Coordination number, σ^2--Debye-Waller factor, R_f--The residual factor is a measure of the mismatch between theoretical and experimental Fourier-filtered spectra. Values in italics denote parameters that are fixed during the fitting procedures.

Figure Captions

Figure 1 Sorption isotherms of Eu(III) in the γ-Al_2O_3/Eu(III) systems. t=2 *d*, pH=6.5, m/V=0.5 g/L, *I*=0.01 mol/L $NaNO_3$.

Figure 2 XRD patterns of the γ-Al_2O_3 samples soaked in the solution with different temperatures.

Figure 3 The relative proportion of Eu(III) species in the solution with different temperatures. $C_{Eu(III)initial}$=5.0×10^{-5} mol/L, *I*=0.01 mol/L $NaNO_3$.

Figure 4 Sorption isotherms of Eu(III) in the γ-Al_2O_3/HA/Eu(III) systems. t=2 *d*, pH=6.5, m/V=0.5 g/L, C_{HA}=10 mg/L, *I*=0.01 mol/L $NaNO_3$.

Figure 5 Sorption isotherms of HA in the γ-Al_2O_3/HA systems. t=2 *d*, pH=6.5, m/V=0.5 g/L, *I*=0.01 mol/L $NaNO_3$.

Figure 6 Sorption percentage of Eu(III) in the γ-Al_2O_3/HA/Eu(III) systems under different contact orders. *T*=293 K, pH=6.5, m/V=0.5 g/L, $C_{Eu(III)initial}$=5.0×10^{-5} mol/L, C_{HA}=10 mg/L, *I*=0.01 mol/L $NaNO_3$.

Figure 7 Zeta potentials of the γ-Al_2O_3 in the absence and presence of HA. *T*=293 K, m/V=0.5 g/L, C_{HA}=10 mg/L, *I*=0.01 mol/L $NaNO_3$.

Figure 8 The k^3-weighted EXAFS spectra and the RSFs of Eu(III) sorption samples prepared in the γ-Al_2O_3/Eu(III) systems at different temperatures. (A) Solid lines represent the k^3-weighted EXAFS spectra; (B) Symbols represent the experimental RSF magnitudes and solid lines represent the spectral fits. t=2 *d*, pH=6.5, m/V=0.5 g/L, $C_{Eu(III)initial}$=5.0×10^{-5} mol/L, *I*=0.01 mol/L $NaNO_3$.

Figure 9 Schematic illustrations of the binding modes of Eu(III) on γ-Al_2O_3 in the absence and presence of HA.

Figure 10 The k^3-weighted EXAFS spectra and the RSFs of Eu(III) sorption samples prepared in

the ternary γ-Al_2O_3/HA/Eu(III) systems at different temperatures. (A) Solid lines represent the k^3-weighted EXAFS spectra; (B) Symbols represent the experimental RSF magnitudes and solid lines represent the spectral fits. t=2 *d*, pH=6.5, m/V=0.5 g/L, $C_{Eu(III)initial}$=5.0×10^{-5} mol/L, C_{HA}=10 mg/L, *I*=0.01 mol/L $NaNO_3$.

Figure 11 The k^3-weighted EXAFS spectra and the RSFs of Eu(III) sorption samples prepared in the γ-Al_2O_3/HA/Eu(III) systems under different contact orders. (A) Solid lines represent the k^3-weighted EXAFS spectra; (B) Symbols represent the experimental RSF magnitudes and solid lines represent the spectral fits. *T*=293 K, pH=6.5, m/V=0.5 g/L, $C_{Eu(III)initial}$=5.0×10^{-5} mol/L, C_{HA}=10 mg/L, *I*=0.01 mol/L $NaNO_3$.

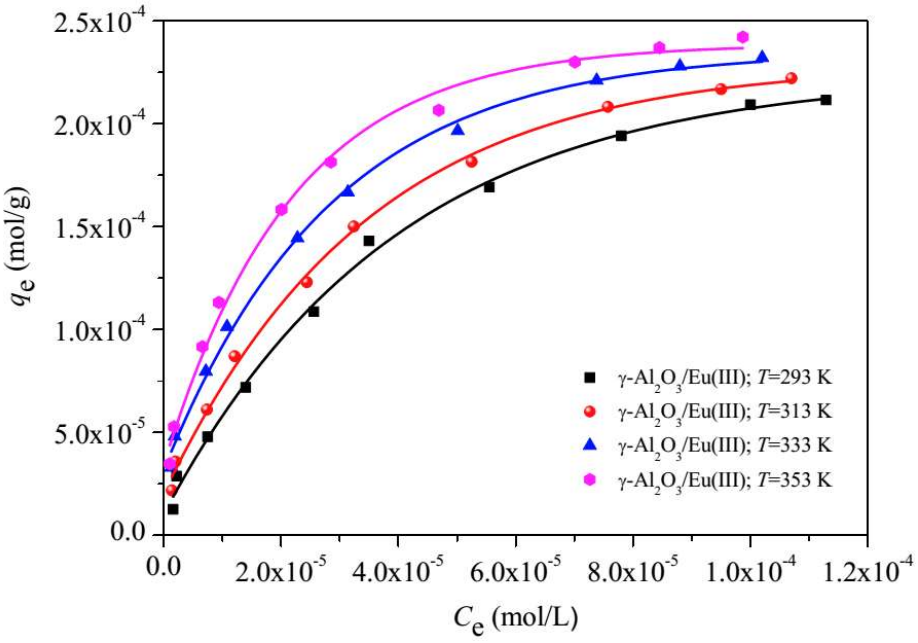

Figure 1

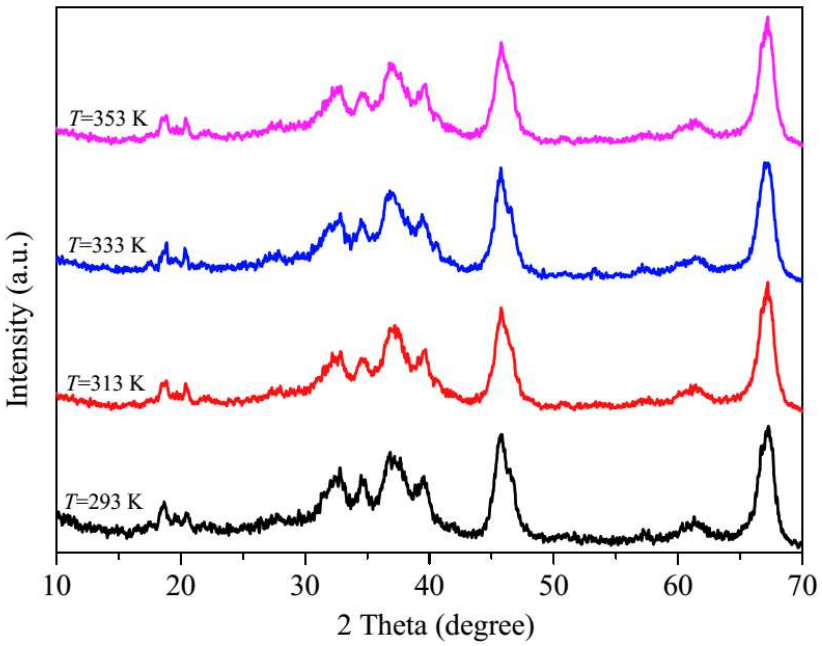

Figure 2

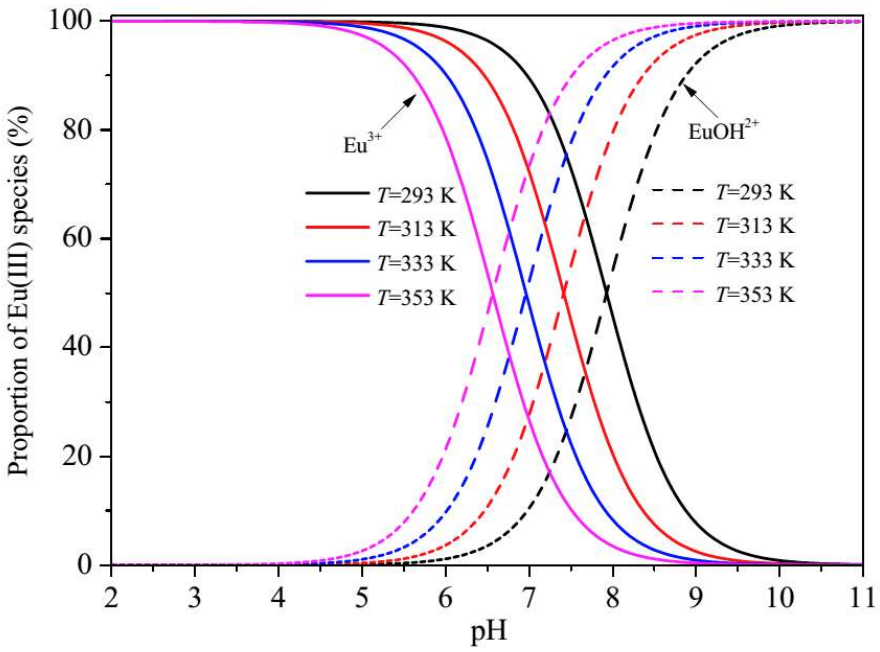

Figure 3

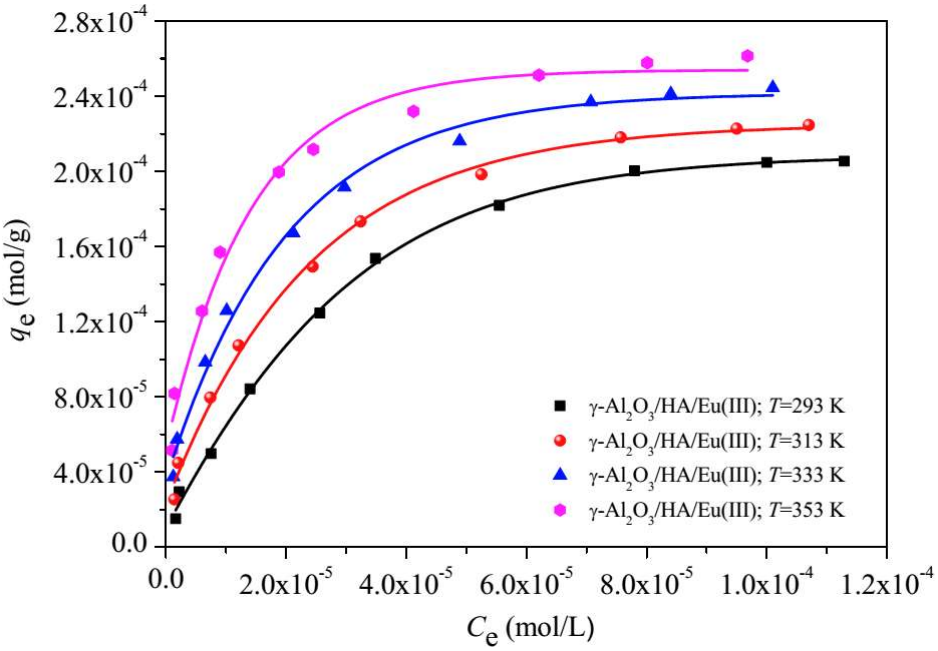

Figure 4

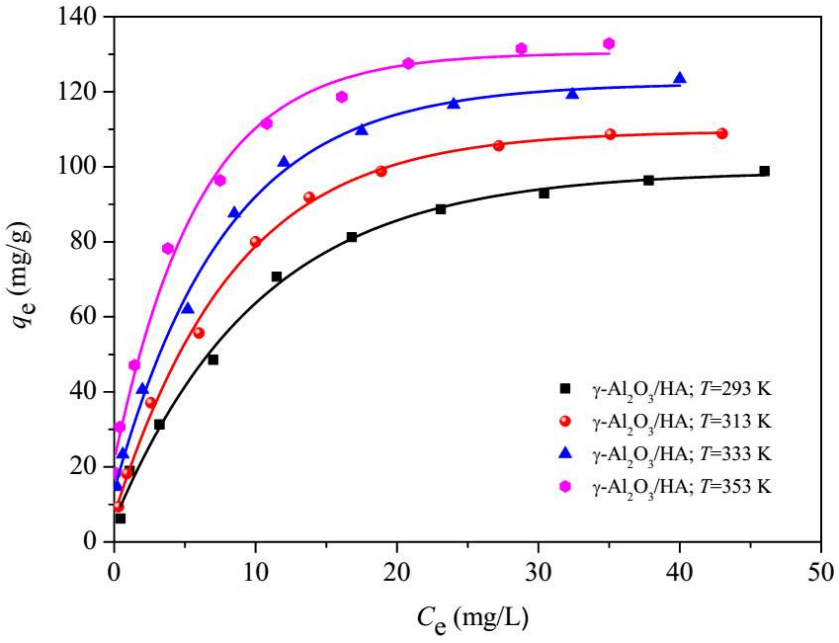

Figure 5

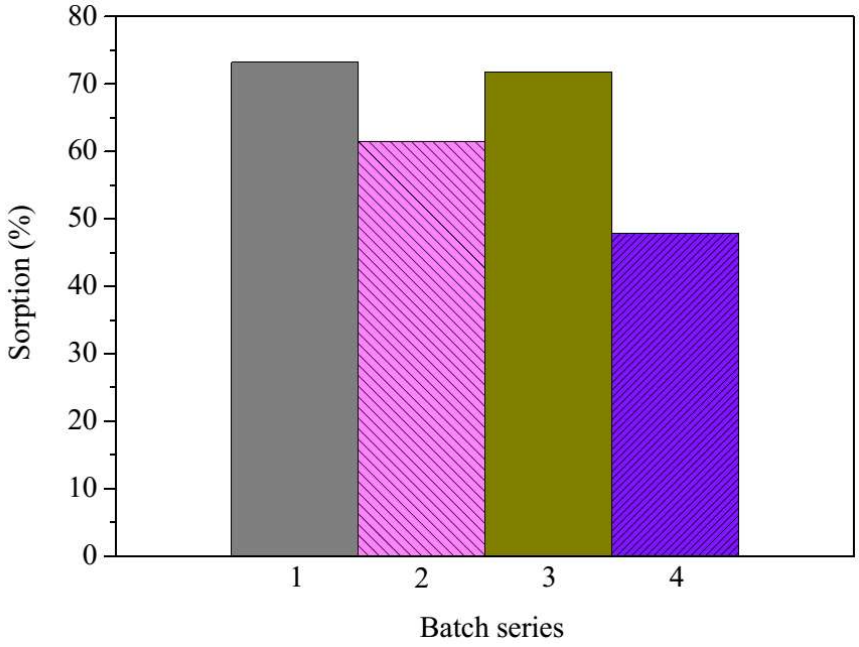

Figure 6

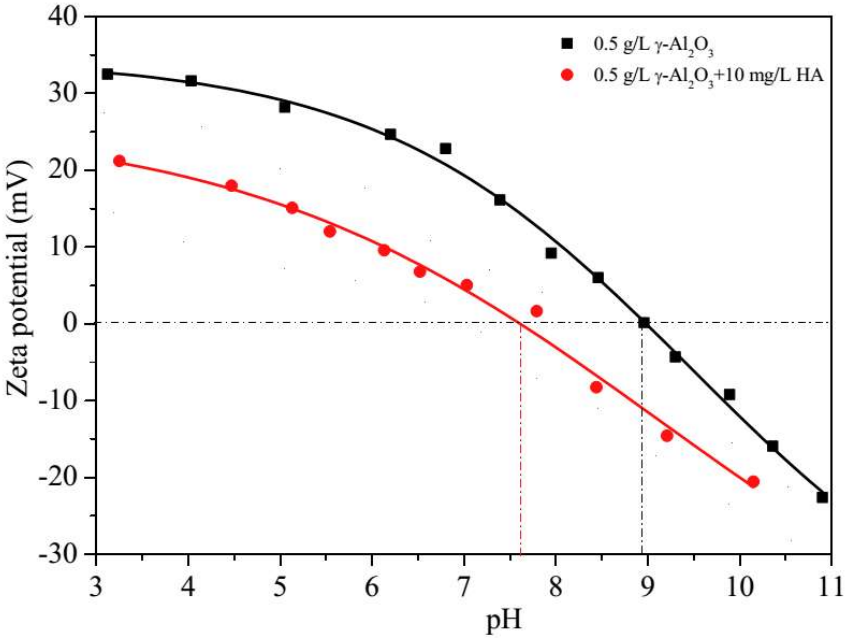

Figure 7

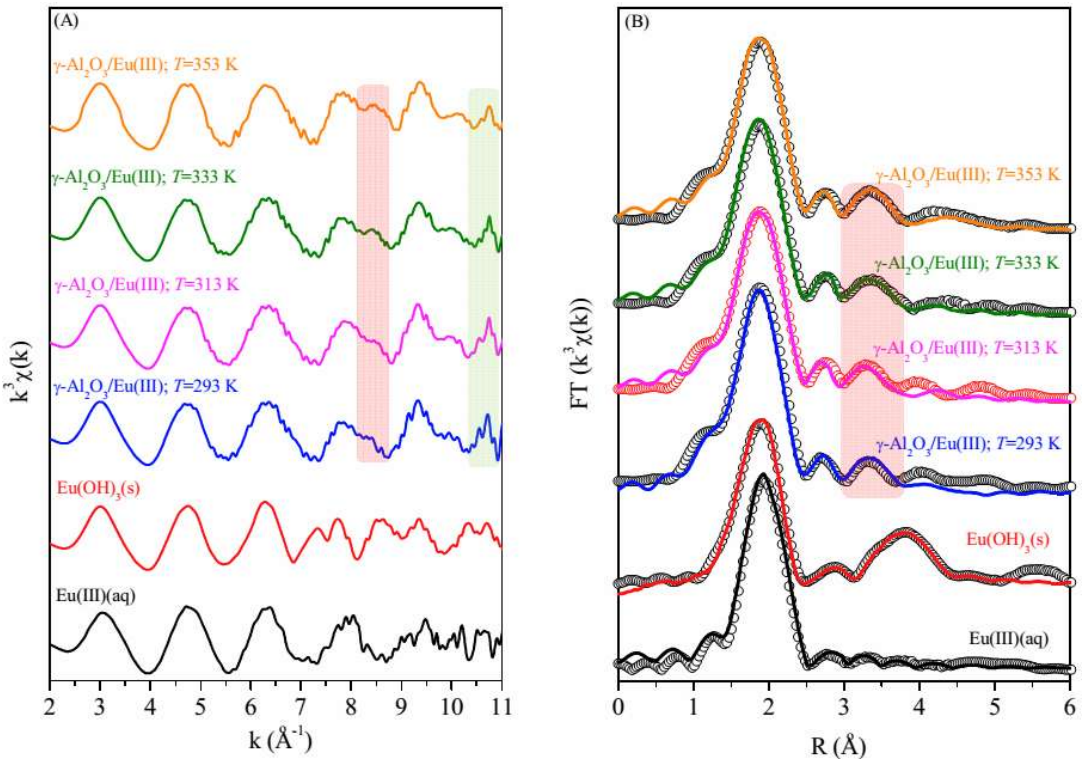

Figure 8

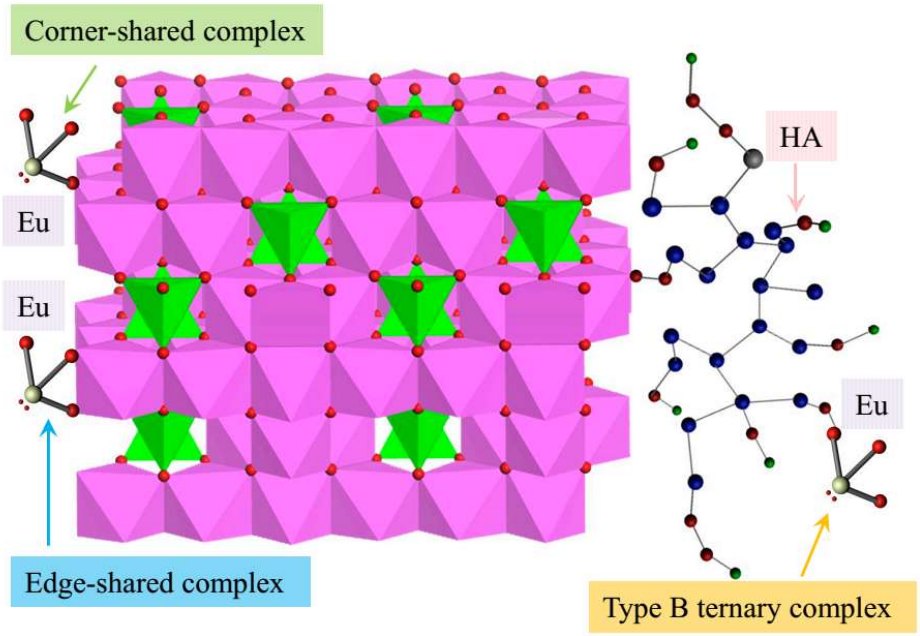

Figure 9

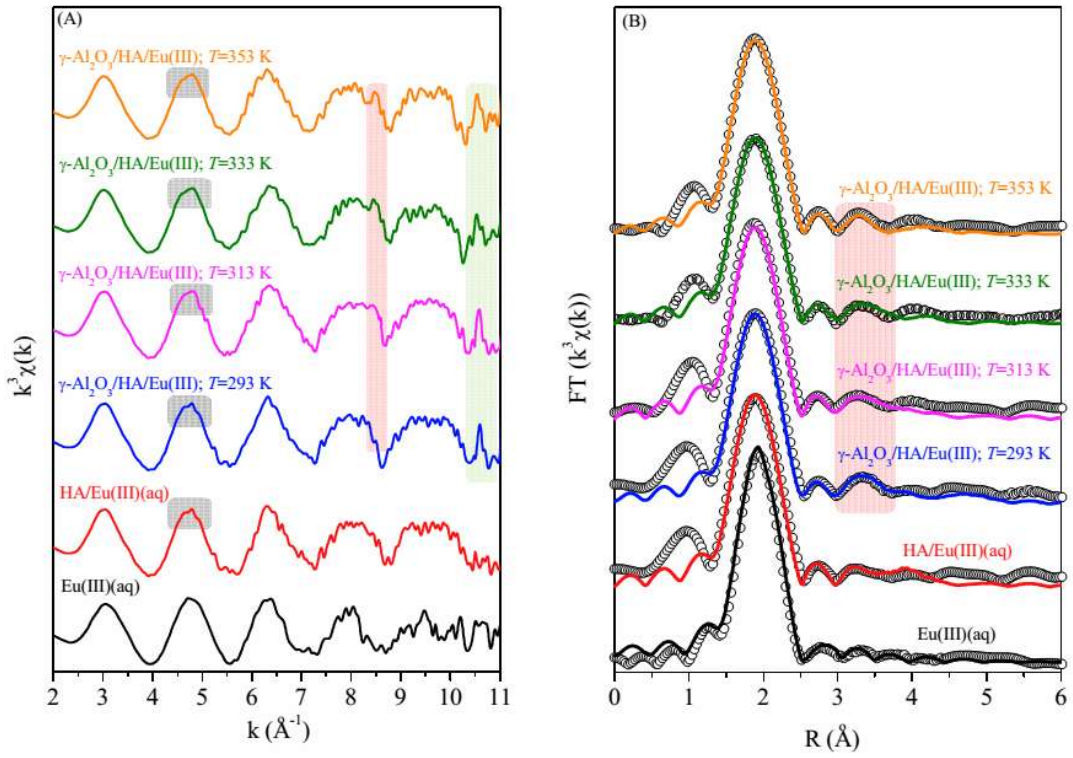

Figure 10

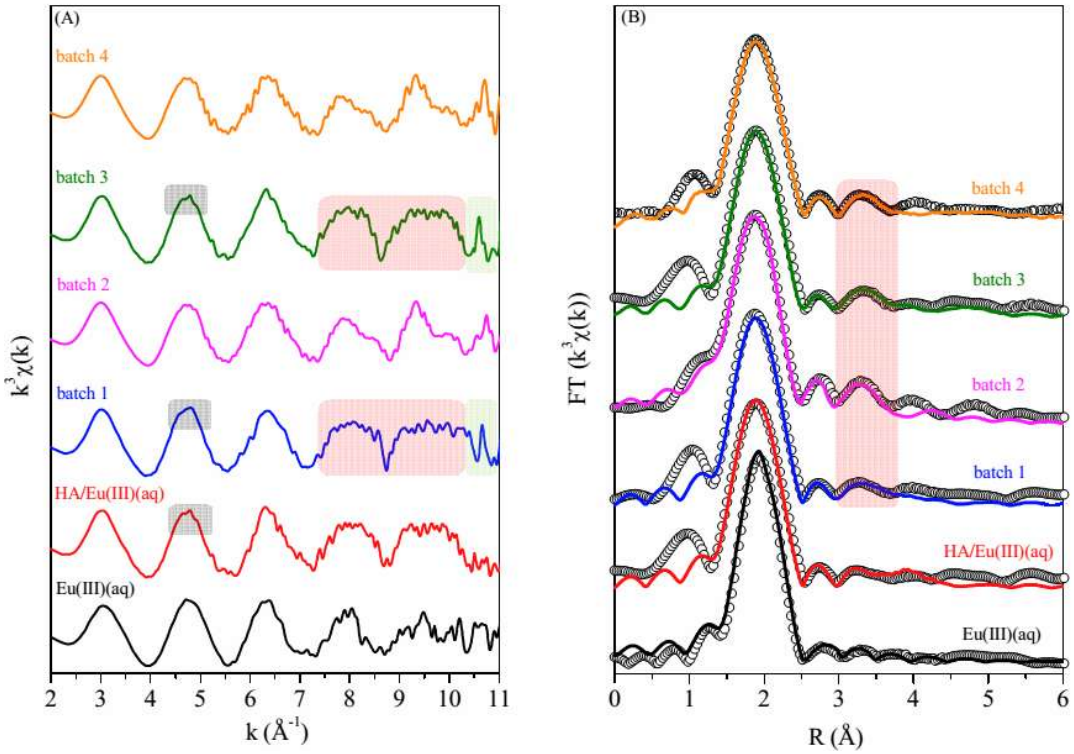

Figure 11